ACS OMEGA

http://pubs.acs.org/journal/acsodf

Article

Numerical Study on Rotor Cooling of Turbine in Supercritical Carbon Dioxide Cycle

Peng Jiang, Yong Tian, Bo Wang,* and Chaohong Guo

Cite This: *ACS Omega* 2022, 7, 39325−39334

Read Online

ACCESS | Metrics & More | Article Recommendations

ABSTRACT: The supercritical carbon dioxide cycle is a Brayton cycle with great application prospects. As a key equipment in this cycle, the turbine machinery usually adopts a dry gas seal as the sealing method between the cylinder and sliding bearing to reduce the leakage of carbon dioxide. In this paper, the numerical model of supercritical carbon dioxide turbine rotor cooling is established, and the grid independence is verified. The effects of inlet temperature and flow rate of dry gas seal and leakage flow rate from cylinder to dry gas seal at the high-temperature inlet side of a turbine upon rotor cooling are studied. The effects of inlet temperature T_{in} and flow rate Q_v of sealing gas in a dry gas seal and leakage mass flow rate Q_m from a cylinder to dry gas seal on pressure loss, outlet flow distribution, exhaust temperature, and rotor temperature distribution are analyzed. As a result, it can be found that with the increase of the inlet flow rate of dry gas seal gas and the leakage flow rate from cylinder to dry gas seal, the pressure difference between the inlet and outlet of each seal gas increases. When the inlet flow rate of dry gas seal gas ranges from 300 N m^3/h to 900 N m^3/h, with the leakage flow from cylinder to dry gas seal increasing from 1.3 kg/s to 2.08 kg/s, the pressure difference between inlet and outlet of each seal gas increases by 7.9% to 13.4%. The pressure difference between the inlet and outlet of each seal gas decreases with the increase of the inlet temperature of dry gas seal gas. When the inlet flow rate of the seal gas of the dry gas seal is 300 N m^3/h and the leakage flow rate from cylinder to dry gas seal is 2.08 kg/s, the inlet temperature of seal gas increases from 100 to 150 °C, and the flow distribution at the outlet is basically unchanged. The research provides theoretical reference for rotor cooling design of a supercritical carbon dioxide turbine.

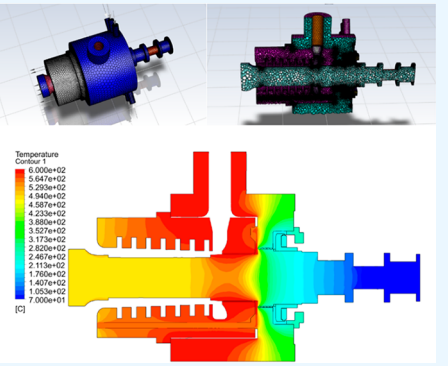

1. INTRODUCTION

Energy and environmental problems are becoming more and more prominent. In recent years, researchers have tried to find a more effective conversion system or power cycle to replace an existing system or power cycle, so as to improve energy efficiency. Feher designed the first supercritical carbon dioxide (s-CO_2) cycle in 1967, which has a small volume and high efficiency, and is a promising cycle mode that can replace existing cycles.[1,2]

At the same time, scientists are exploring more applications of the supercritical carbon dioxide cycle, and improving the efficiency of the system through analysis and optimization.[3−5] Mohammadi et al.[3] proposed a novel triple power cycle where waste heat from a gas turbine cycle is utilized to drive a supercritical carbon dioxide (s-CO_2) recompression cycle and a recuperative organic Rankine cycle (ORC) in sequence. They developed a detailed thermoeconomic model in MATLAB to evaluate the performance of the proposed cycle under different operating conditions. A detailed analysis and optimization study of the recompression cycle were presented by Saeed and Kim.[4] A recompression sCO_2 cycle for a solar central particles receiver application was optimized by Reyes-Belmonte et al.,[5] and the net cycle efficiency is close to 50%.

The application of supercritical carbon dioxide cycle is inseparable from the development and design of key equipment. The development of a high-efficiency supercritical carbon dioxide turbine is still in the design and optimization stage, and researchers are trying to study the design method and improve its efficiency.[6−10] Zhou et al.[6] proposed and designed a 1.5-MW S-CO_2 radial inflow turbine. The three-dimensional (3D) numerical simulation of the designed turbine is carried out by using ANSYS-CFX commercial software, and the results are in good agreement with the design values. The aerothermodynamic design, blade geometrical design, CFD analysis results, and strength evaluation of 15-MW axial SCO_2 turbine and 1.5-MW radial SCO_2 turbine were investigated by Zhang et al.[7] Uusitalo and Grönman[8] investigated the losses of supercritical CO_2 radial turbines with design power scales of about 1 MW using computational

Received: August 27, 2022
Accepted: October 12, 2022
Published: October 20, 2022

https://doi.org/10.1021/acsomega.2c05531
ACS Omega 2022, 7, 39325−39334

fluid dynamic simulations and found a similar trend in the development of the losses as the turbine specific speed was changed. CFD analysis of a supercritical carbon dioxide (SCO_2) radial-inflow turbine generating 100 kW from a concentrated solar resource of 560 °C with a pressure ratio of 2.2 was explored by Odabaee et al.[9] Luo et al.[10] designed a 10 MW single-stage centrifugal turbine using SCO_2 as the working fluid and obtained the SCO_2 centrifugal steam turbine with total static efficiency and output power of 89.02% and 10.07%.

Different from the traditional steam cycle, the leakage of carbon dioxide in a supercritical carbon dioxide cycle should be minimized. At present, a dry gas seal with small leakage is widely used in compressors and turbines as the shaft end seal of equipment. A lot of research work has been done on the structure and performance of dry gas seal.[11−22]

Theoretical calculations and experimental tests were performed to investigate the influence of turbulence effect and different flow processes on S-CO_2 dry gas seal performance by Yan et al.[11] Thatte et al.[12] quantified the effect of various design features on the optimal performance and provided insights for a successful dry gas seal operation in a sCO_2 turbomachine. The chamber temperature, cooling effects, and the deformation of the rotating ring were numerically investigated using the fluid-thermal-solid coupling by Yuan et al.,[13] and it was found that the designed tangential admission cooling structure has the best cooling performance. Laxander et al.[14] gave insight into the seal and test loop design, the test campaign, and results. The effects of different fluids, rotational speeds, pressure ratios, and whirl types on seal dynamic characteristics were compared and analyzed by Si et al.[15] The effect of grooved ring rotation on sealing performance was discussed by Du et al.[16] The sealing performance of the SCO_2 model is more easily affected by the inlet temperature and pressure compared with the air model. Muhammad et al.[17] proposed a new barrier gas method to reduce the power associated with the leakage supplement system for the sCO_2 turbine and reduced the leakage flow rate from the turbine. Wu et al.[18] studied the sealing characteristics of the single-stage spiral groove dry gas seal in the SCO_2 operating environment and found that the dry gas seal leakage flow rate under different film thicknesses is 0.04% to 0.45% of the SCO_2 compressor flow rate. Zakariya and Jahn[19] investigated the supercritical CO_2 dry gas seals operating close to the critical point with an inlet pressure and temperature of 8.5 MPa and 370 K, respectively, and a speed of 30000 rpm and presented the effects of the groove length or dam to groove ratio on the performance of the dry gas seal. Du and Zhang[20] investigated the performance of supercritical CO_2 dry gas seal with a different deep spiral groove and found that SCO_2 DGS can generate larger average film pressure, open force, and leakage with lower average face temperature than air DGS. Fairuz Zakariya[21] optimized the face geometry for a small to median scale supercritical closed loop Brayton cycle (1−20 MWe). Fairuz et al.[22] conducted coupled simulations to explore trends and methods to reduce the distortion of a dry gas seal operating with supercritical CO_2.

The Brayton cycle is adopted in the supercritical carbon dioxide cycle test bed. Different from the traditional power plant, it is a closed cycle, so it is necessary to reduce the leakage of the system. In this cycle, a dry gas seal is used for compressor and turbine equipment. Because the use of a dry gas seal is limited by temperature, and the inlet temperature of the turbine is as high as 600 °C, the design of a high-temperature turbine is difficult, especially for the rotor cooling between the turbine inlet and dry gas seal. If the dry gas seal can work normally, the rotor temperature at the installation position of dry gas seal must be reduced to the service temperature, and the rotor length should be controlled to ensure reliable rotor dynamics and compact turbine structure. It is helpful for the design of supercritical carbon dioxide turbine structure and determination of cooling flow rate to study the influence of the temperature and flow rate of dry gas seal sealing gas and the flow rate of the turbine main flow leaking to the dry gas seal on the cooling effect of the turbine.

The supercritical carbon dioxide cycle test-bed[23] is being built in Shanghai Lingang District, and the schematic diagram of supercritical carbon dioxide cycle test-bed is shown in Figure 1. In this paper, the numerical model of the supercritical carbon dioxide turbine rotor cooling is established, and the grid independence is verified in section 2. The effects of inlet temperature and flow rate of dry gas seal and leakage flow rate from cylinder to dry gas seal at high temperature inlet side of the turbine on rotor cooling are studied. The effects of inlet temperature T_{in} and flow rate Q_v of the sealing gas in the dry gas seal and leakage mass flow rate Q_m from cylinder to dry gas seal on the pressure loss, outlet flow distribution, exhaust temperature, and rotor temperature distribution are analyzed. The results are presented in section 3. Finally, a summary of the present work is presented in section 4.

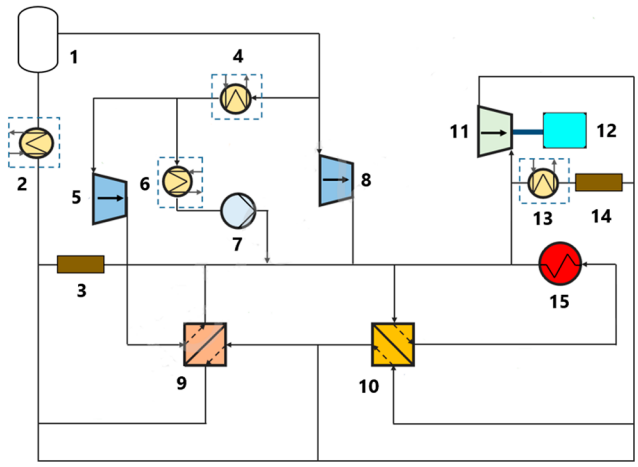

Figure 1. Schematic diagram of supercritical carbon dioxide cycle test-bed: 1, buffer tank; 2 and 13, cooler; 3 and 14, reliever; 4, precooler; 5, main compressor; 6, condenser; 7, pump; 8, recompressor; 9, low temperature recuperator; 10, high temperature recuperator; 11, turbine; 12, power consuming machine; 15, heater.

2. NUMERICAL CALCULATION MODEL AND METHOD

2.1. Physical Model. Inlet temperature of supercritical carbon dioxide turbine is 600 °C, inlet pressure is 23.2 MPa, inlet flow rate is 26 kg/s, exhaust pressure is 9.3 MPa, and exhaust temperature is 495 °C. The geometric model of the dry gas seal cooling calculation is shown in Figure 2. The geometric model not only considers the asymmetry of the turbine structure, but also simplifies the model reasonably to minimize the calculation error. The geometric model used for calculation simplifies the turbine structure, ignoring the blade shape of the turbine and the structure of the outlet. There are six inlets for dry gas seal cooling gas. The cooling gas is mixed with the cylinder leakage gas, and then mixed with the turbine

https://doi.org/10.1021/acsomega.2c05531
ACS Omega 2022, 7, 39325−39334

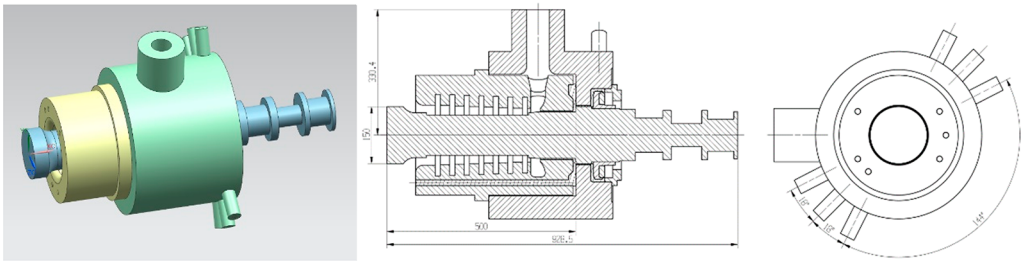

Figure 2. Geometric model.

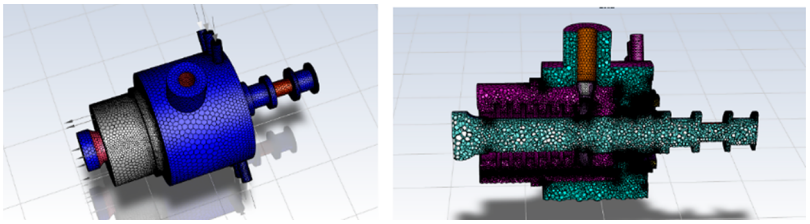

Figure 3. Mesh model.

exhaust gas at the position of the casing near the turbine outlet, and then discharged. The top clearance of comb seal between cylinder and dry gas seal is 0.3 mm.

2.2. Numerical Calculation Method. The steady compressible Navier Stroke equations are given by the following.[24]

Conservation of momentum:

$$\frac{\partial}{\partial t}(\rho\vec{v}) + \nabla\cdot(\rho\vec{v}\vec{v}) = -\nabla P + \nabla\cdot(\bar{\bar{\tau}}) \quad (1)$$

where $\bar{\bar{\tau}}$ is the stress tensor given by

$$\bar{\bar{\tau}} = \mu\left[(\nabla\vec{v} + \nabla\vec{v}^{T}) - \frac{2}{3}\nabla\vec{v}I\right] \quad (2)$$

where μ is the molecular viscosity, I is the unit tensor, and the second term on the right-hand side is the effect of volume dilation.

Mass conservation:

$$\frac{\partial\rho}{\partial t} + \nabla\cdot(\rho\vec{v}) = S_m \quad (3)$$

The source S_m is the mass added to the continuous phase from the dispersed second phase and any sources.

Conservation of energy:

$$\frac{\partial}{\partial t}(\rho E) + \nabla\cdot(\vec{v}(\rho E + p)) = -\nabla\cdot\left(\sum_j h_j J_j\right) + S_h \quad (4)$$

As shown in Figure 3, the polyhedral grid is generated by the grid generation software fluent meshing, and the watertight geometry workflow was adopted. The grid is imported into ANSYS fluent to get the solution. The maximum expansion rate of the boundary layer is set to 1.2. As shown in Figure 4, there are 3 boundary layers of grids near the surface of fluid. The mesh number of the model is approximately 15,340,000. As shown in Figure 5, the grid independence of the calculation model is verified. The SST k-omega model is chosen to calculate the flow. The convergence precision of all root-mean-square residuals is less than 10×10^{-5}. The working fluid material is CO_2 and the physical state at the inlet is

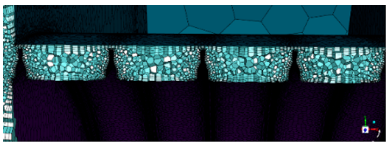

Figure 4. Details of grids in the tip clearance region.

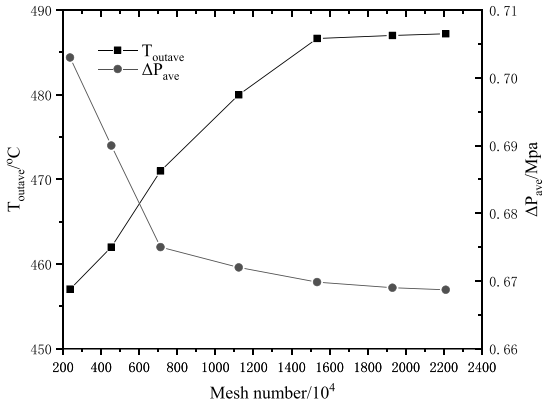

Figure 5. Mesh independency investigation.

supercritical. The carbon dioxide three-phase distribution diagram is shown in Figure 6. In order to accurately simulate

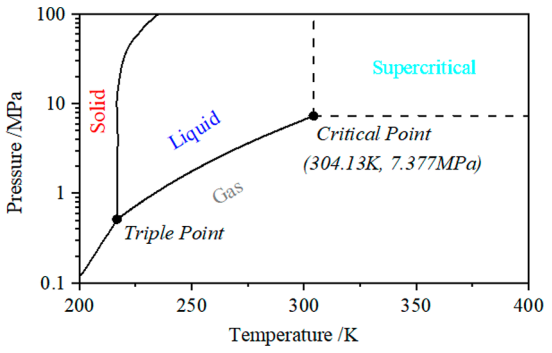

Figure 6. Carbon dioxide three-phase distribution diagram

https://doi.org/10.1021/acsomega.2c05531
ACS Omega 2022, 7, 39325−39334

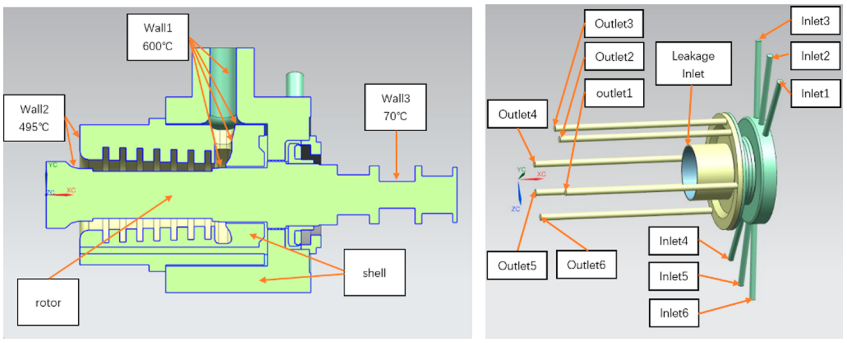

Figure 7. Boundary conditions.

Table 1. Boundary Conditions

no.	n/rpm	Q_m/(kg/s)	Q_v/(Nm^3/h)	T_{in}/°C	T_{wall2}/°C	P_{out}/MPa	T_{wall3}/°C
1	16000	1.3	900	100	495	9.3	70
2	16000	1.3	900	130	495	9.3	70
3	16000	2.08	900	100	495	9.3	70
4	16000	2.08	900	130	495	9.3	70
5	16000	2.08	900	150	495	9.3	70
6	16000	1.3	700	130	495	9.3	70
7	16000	2.08	700	130	495	9.3	70
8	16000	1.3	500	130	495	9.3	70
9	16000	2.08	500	130	495	9.3	70
10	16000	1.3	300	130	495	9.3	70
11	16000	2.08	300	130	495	9.3	70

the real state of CO_2, the physical property database given by NIST[25] is adopted. The NIST database is established by the Span and Wagner (SW) equation, which is interpreted as a fundamental equation of Helmholtz energy equation. The SW equation covers a wide range for pressure and temperature, and holds excellent performance near the critical point, where the accuracy is equivalent to the test uncertainty.[26] The material of rotor and shell is defined as steel.

As shown in Figure 7 and Table 1, the massflow inlet is adopted and the temperature at the leakage inlet is 600 °C. The inlet temperature on the wall1 and wall2 are 600 and 495 °C respectively. The outlet static pressure is 9.3 MPa. The surface temperature of the rotor at the installation position of the bearing is 70 °C, and the rotation speed of the rotor is 16000 rpm The leakage flow Q_m from cylinder to dry gas seal is 1.3 kg/s and 2.08 kg/s, respectively. The total volume flow of dry gas sealing gas ranges from 300 N m^3/h to 900 N m^3/h, and the inlet temperature ranges from 100 to 150 °C.

3. RESULTS AND DISCUSSIONS

3.1. Influence of Inlet Temperature T_{in} and Flow Rate Q_v of Dry Gas Seal Gas and Leakage Flow Rate Q_m from Cylinder to Dry Gas Seal on Pressure Loss. As shown in Figure 8 and Figure 9, there is a pressure difference between the inlet and outlet of each seal gas under different inlet temperatures and flow rates of the seal gas of dry gas seal and the leakage flow rate from cylinder to dry gas seal. With the increase of the inlet flow rate of dry gas seal gas and the leakage flow rate from cylinder to dry gas seal, the pressure difference between the inlet and outlet of each seal gas increases. When the inlet flow rate of dry gas seal gas ranges from 300 N m^3/h to 900 N m^3/h, with the leakage flow from cylinder to dry gas seal increasing from 1.3 kg/s to 2.08 kg/s, the pressure difference between inlet and outlet of each seal gas increases by

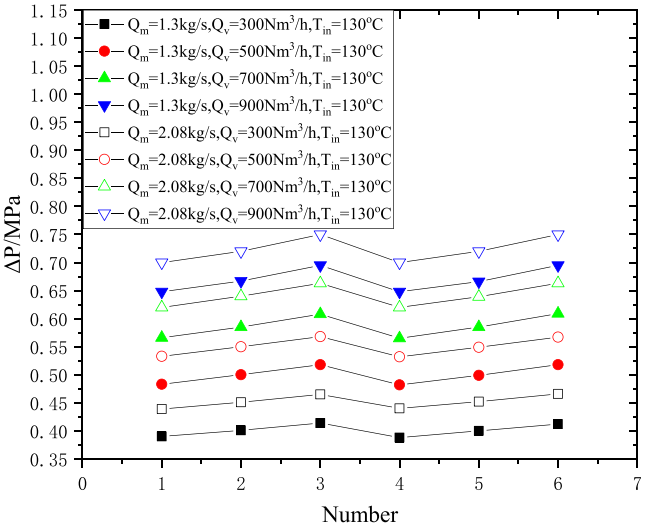

Figure 8. Pressure difference between inlet and outlet under different inlet flow rates of dry gas seal gas and leakage flow from cylinder to dry gas seal.

7.9% to 13.4%. The pressure difference between the inlet and outlet of each seal gas decreases with the increase of the inlet temperature of dry gas seal gas, which is mainly related to the properties of supercritical carbon dioxide. The density increases with the increase of temperature, and the flow rate of carbon dioxide in the channel decreases.

3.2. Influence of Inlet Temperature and Flow Rate of Dry Gas Seal Gas and Leakage Flow Rate from Cylinder to Dry Gas Seal on Outlet Flow Distribution. The mass flow distribution of each seal gas outlet is shown in Figure 10 and Figure 11 under different inlet temperature, flow rate, and leakage flow rate from cylinder to dry gas seal. When the inlet

https://doi.org/10.1021/acsomega.2c05531
ACS Omega 2022, 7, 39325−39334

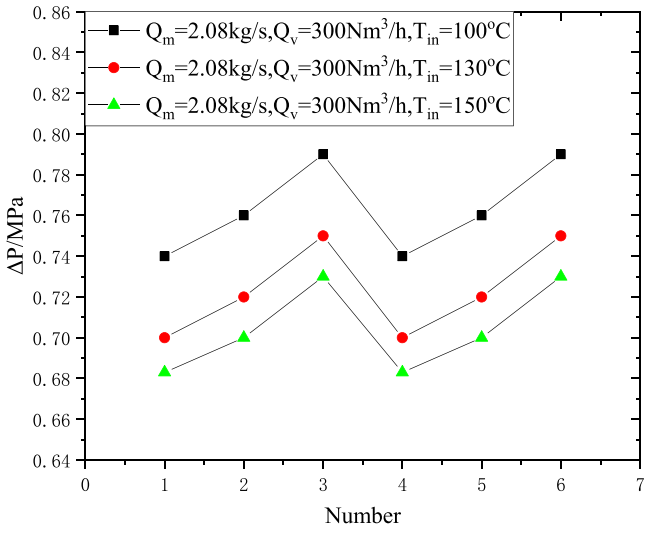

Figure 9. Pressure difference between inlet and outlet of dry gas seal at different inlet temperatures.

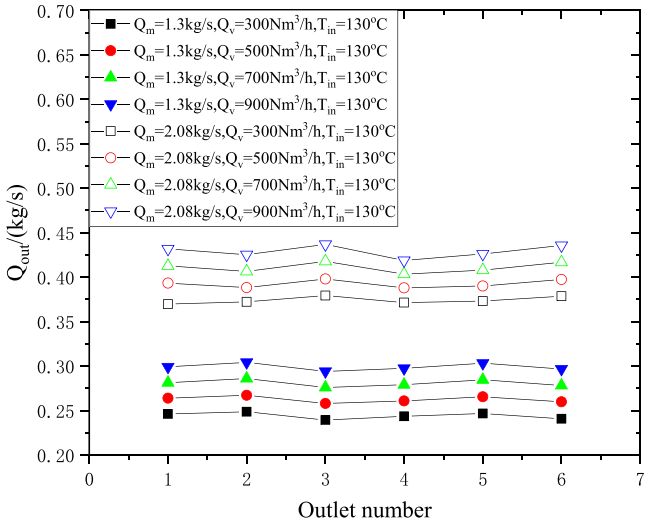

Figure 10. Outlet flow under different inlet flow rates of dry gas seal gas and leakage flow rates from cylinder to dry gas seal.

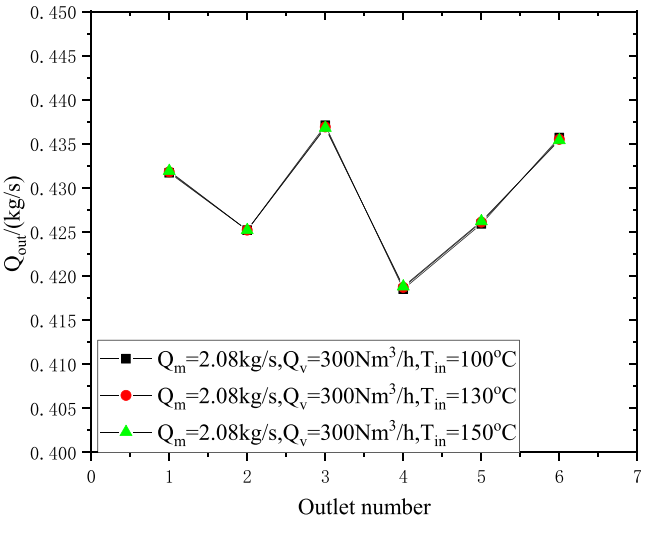

Figure 11. Outlet flow rate at different inlet temperatures of dry gas seal gas.

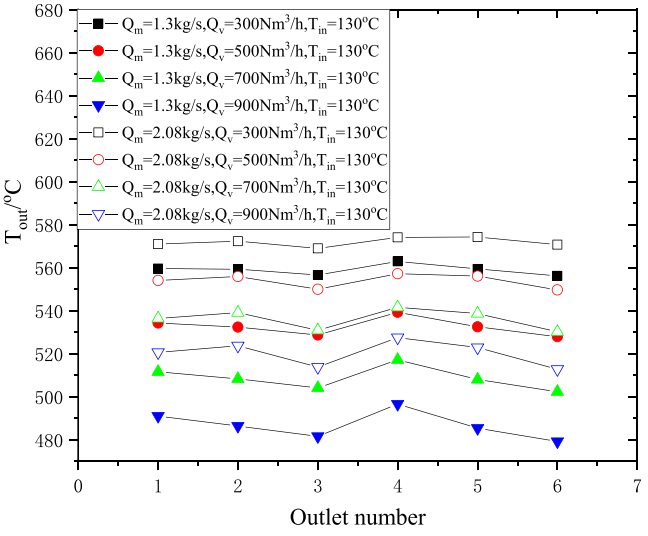

Figure 12. Outlet temperature under different inlet flow rates of dry gas seal gas and leakage flow rates from cylinder to dry gas seal.

flow of seal gas is evenly distributed, the outlet flow distribution is not exactly the same, mainly because of the uneven distribution of inlet and outlet and the uneven distribution of temperature. When the inlet flow rate of seal gas of dry gas seal is 300 N m^3/h and the leakage flow rate from cylinder to dry gas seal is 2.08 kg/s, the inlet temperature of seal gas increases from 100 to 150 °C, and the flow distribution at the outlet is basically unchanged. It is mainly because the flow rate of sealing gas is much smaller than the leakage flow rate from cylinder to dry gas seal, and the flow rate of sealing gas is less than one tenth of the leakage flow rate.

3.3. Influence of Inlet Temperature and Flow Rate of Dry Gas Seal Gas and Leakage Flow Rate from Cylinder to Dry Gas Seal on Exhaust Temperature. Under different inlet temperatures, flow rates of dry gas seals and leakage flow rates from cylinders to dry gas seals, the mass temperature distribution of each seal gas outlet is shown in Figure 12 and Figure 13. When the inlet temperature of sealing gas and the leakage flow from cylinder to dry gas seal are constant, the outlet temperature decreases with the increase of the inlet flow of sealing gas. Within the range of 300 N m^3/h-900 N m^3/h, the average outlet temperature increases by 3.2%−4.7% for every 200 N m^3/h increase in the inlet flow. The inlet temperature of the seal gas is lower than the temperature of the leakage gas from the cylinder to the dry gas seal. With the increase of the inlet flow rate, the proportion of the inlet flow rate to the total flow rate increases, and the temperature after the mixture of the two decreases. The outlet temperature increases with the increase of leakage flow from cylinder to dry gas seal. As the leakage flow to the cylinder dry gas seal increases, the proportion of intake flow to the total flow decreases, and the temperature after the mixture of the two increases.

The outlet temperature rises with the increase of the inlet temperature of the sealing gas, and the outlet temperature rises by 3−6 °C for every 20 °C increase in the inlet temperature.

3.4. Influence of the Temperature and Flow Rate of Dry Gas Seal Gas and the Leakage Flow Rate from Cylinder to Dry Gas Seal on the Average Temperature

https://doi.org/10.1021/acsomega.2c05531
ACS Omega 2022, 7, 39325−39334

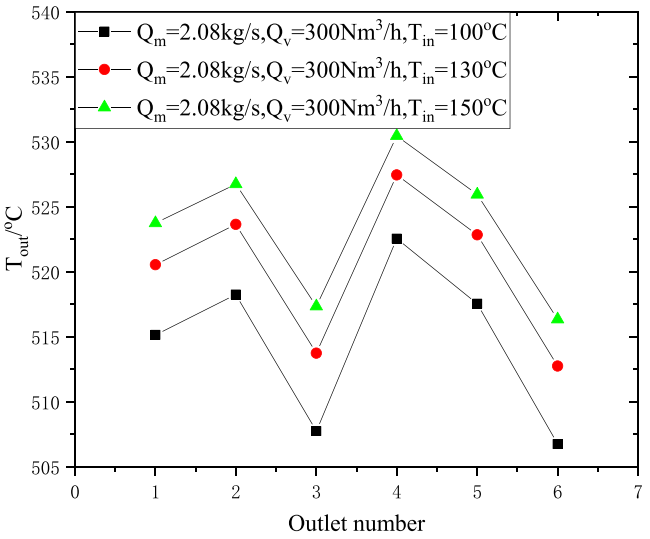

Figure 13. Outlet temperature at different inlet temperatures of dry gas seal.

of Rotor Section. The average temperature distribution of the rotor section along the axial direction is shown in Figure 14

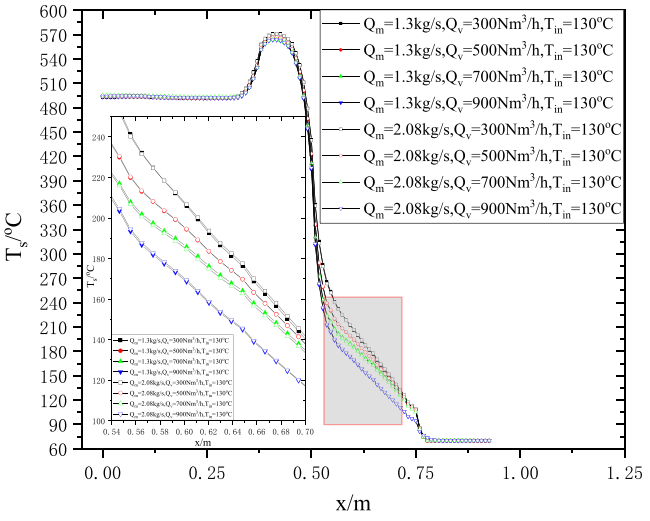

Figure 14. Average temperature of rotor section under different inlet flow rates of dry gas seal gas and leakage flow rates from cylinder to dry gas seal.

and Figure 15. The leakage flow from cylinder to dry gas seal increases from 1.3 kg/s to 2.08 kg/s, and the average temperature of rotor section changes little. The inlet temperature and flow rate of dry gas seal have great influence on the temperature of local areas, especially between the inlet of dry gas seal and the inlet of leakage gas. As the flow rate of seal gas increases, the average temperature of cross section decreases obviously, and at the same time, the average temperature of cross section decreases with the decrease of the inlet temperature of sealing gas. At the cross-section position x = 0.4 m, the average cross-section temperature of the rotor is the highest, reaching 564 °C. Mainly because this section is close to the high temperature inlet of the turbine, and the inlet CO_2 temperature is 600 °C. At the same time, the average cross-section temperature of the rotor is basically unchanged from the cross-section position x = 0 m to x = 0.3

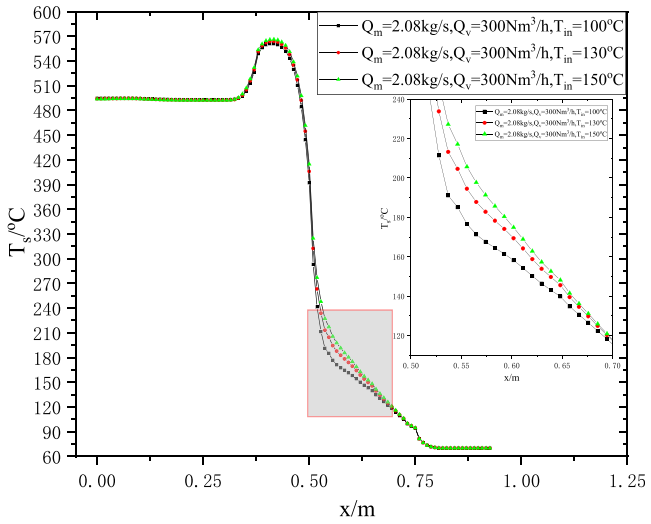

Figure 15. Average temperature of rotor section at different inlet temperatures of dry gas seal gas.

m. The section average temperature of the rotor in this position range is more obviously affected by the turbine outlet temperature. In the range of cross-section position from x = 0.4 m to x = 0.76 m, the average temperature of the rotor cross-section is the highest and decreases rapidly with the cooling of dry gas seal gas.

3.5. Influence of Inlet Temperature and Flow Rate of Dry Gas Seal Gas and Leakage Flow Rate from Cylinder to Dry Gas Seal on Rotor Wall Temperature. The average temperature distribution of the rotor wall along the axial direction is shown in Figure 16 and Figure 17. The leakage

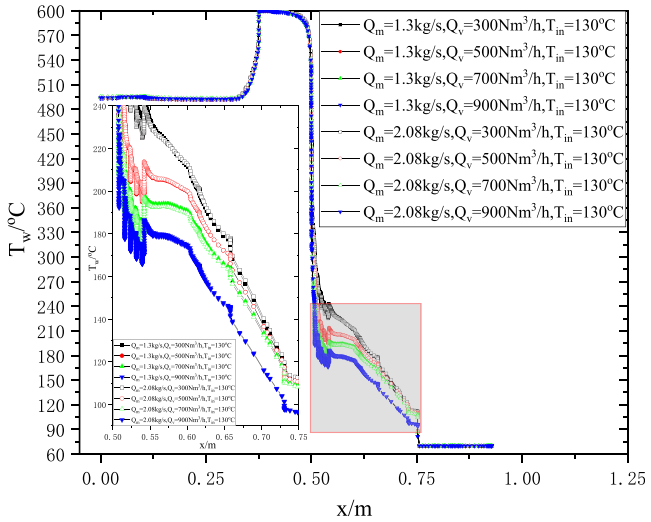

Figure 16. Average temperature of rotor wall under different inlet flow rates of dry gas seal gas and leakage flow rates from cylinder to dry gas seal.

flow rate to the cylinder dry gas seal increases from 1.3 kg/s to 2.08 kg/s, and the average temperature of the rotor wall changes little. The inlet temperature and flow rate of the dry gas seal have a great influence on the rotor temperature of local areas, especially between the dry gas seal inlet and the leakage gas inlet. With the increase of the seal gas flow rate, the average wall temperature decreases obviously, and at the same time, the average wall temperature decreases with the decrease of the

https://doi.org/10.1021/acsomega.2c05531
ACS Omega 2022, 7, 39325−39334

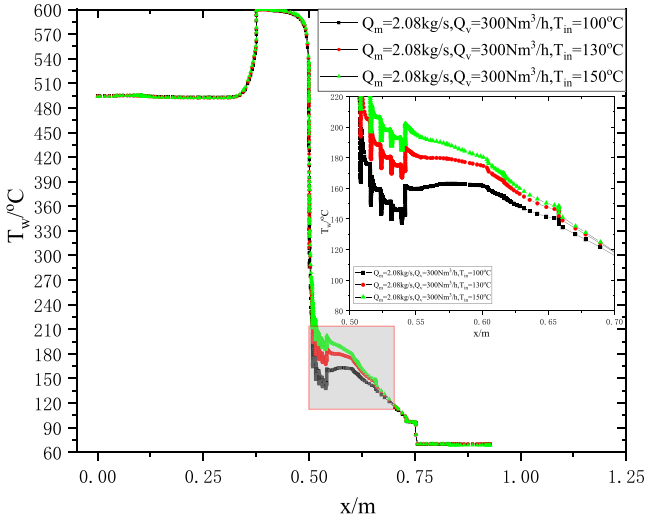

Figure 17. Average temperature of rotor wall under different inlet temperatures of dry gas seal gas.

inlet temperature of the seal gas. The average temperature of the wall began to decrease at the inlet of the leakage gas, and suddenly increased at the position of x = 0.5 m. Because of the presence of the shaft shoulder at this position, the velocity of the high-temperature leakage gas made an angle of 90 with the wall, which was affected by the convective heat transfer of the high-temperature leakage gas, resulting in a higher average temperature of the wall at this position.

3.6. Influence of Temperature T_s and Flow Rate Q_v of Dry Gas Seal Gas and the Leakage Flow Rate Q_m from Cylinder to Dry Gas Seal on the Contact Surface Temperature between Dry Gas Seal and Rotor. As shown in Figure 18 and Figure 19, the average and maximum temperature of the contact surface between dry gas seal and rotor decreases with the increase of sealing gas flow, increases with the increase of leakage flow from cylinder to dry gas seal, and increases with the increase of sealing gas inlet temperature. With the increase of the leakage gas flow rate, more heat is conducted from the high temperature side per unit time, which

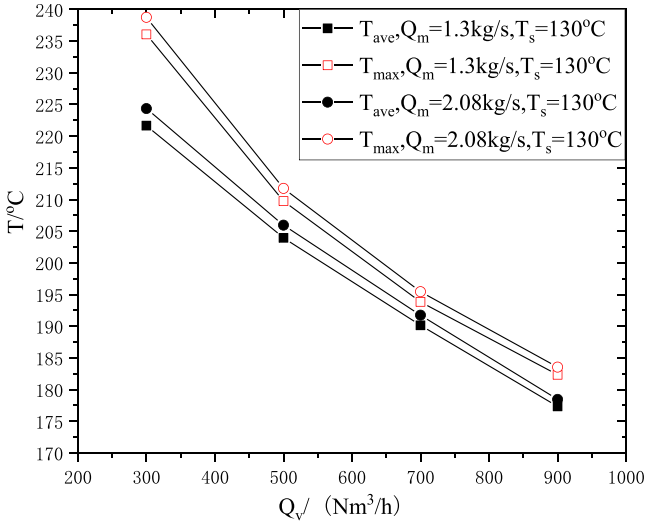

Figure 18. Temperature of contact surface between dry gas seal and rotor under different inlet flow rates of dry gas seal and leakage flows rate from cylinder to dry gas seal.

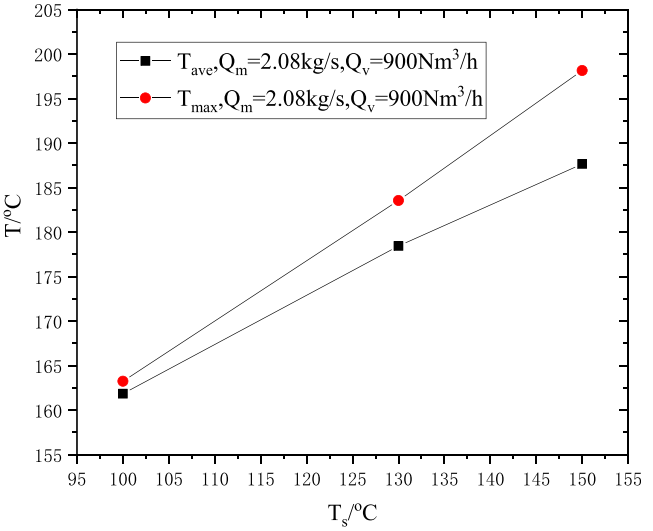

Figure 19. Temperature of contact surface between dry gas seal and rotor at different inlet temperatures of dry gas seal gas.

reduces the cooling effect of dry gas sealing gas on the rotor. The larger is the flow rate and the is lower the inlet temperature of dry gas seal cooling gas, the better is the cooling effect on the rotor.

3.7. Cloud Image and Vector Image. As shown in Figure 20, the temperature cloud chart at the section z = 0 m shows

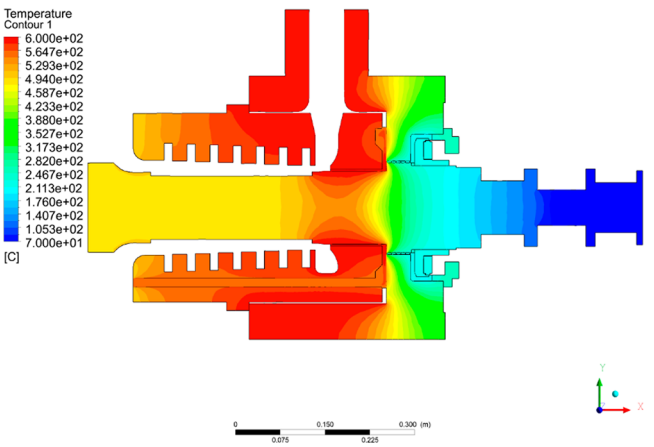

Figure 20. Temperature nephogram at section z = 0 m.

that the bearing position wall1 has the lowest temperature, the cylinder inlet wall wall3 has the highest temperature, and the temperature at the section near the cylinder inlet on the shaft is obviously higher than that at other positions, indicating that the dry gas seal cooling gas has obvious cooling effect on the shaft. The high temperature zone of the rotor is distributed in a small range near the turbine inlet, mainly because the right side of the rotor is cooled by dry gas seal cooling gas, and the left side of the rotor is affected by the turbine outlet temperature.

The velocity vector diagram of the fluid cross section at z = 0 m is shown in Figure 20. As shown in Figure 21, the cylinder leakage gas and the dry gas seal cooling gas are mixed at the outlet of the comb seal, and they are fully mixed in the mixing chamber. After redistribution, they flow through the outlet channel and enter the outlet position of the cylinder, and then they are mixed with the exhaust gas of the cylinder. The obvious backflow occurred in the mixing chamber which is an

https://doi.org/10.1021/acsomega.2c05531
ACS Omega 2022, 7, 39325−39334

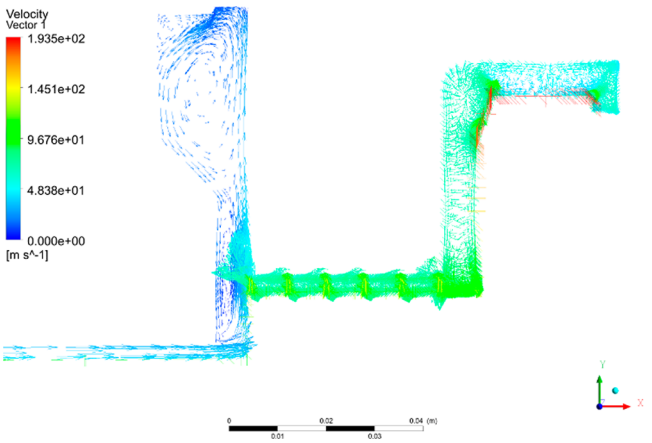

Figure 21. Velocity vector diagram of fluid section z = 0 m.

annular cavity. Because the outlet channel is on the left side of the annular cavity, the mixed gas can not be discharged smoothly, resulting in backflow.

The temperature nephograms of the fluid section at z = 0 m are shown in Figures 21 and 22. As shown in Figure 22 and Figure 23, with the increase of the cooling flow rate of dry gas seal, the area of high temperature section gradually decreases, and the cooling effect is obviously improved: The leakage flow rate to the cylinder dry gas seal increases from 1.3 kg/s to 2.08 kg/s, and the temperature in the mixed area of the leakage gas and the dry gas seal cooling gas increases obviously, but the temperature change in the dry gas seal cooling area is not obvious, which indicates that the comb seal effectively prevented the leakage of the leakage gas to the dry gas seal area. With the increase of inlet temperature of dry gas seal, the temperature in the mixed area of leakage gas and dry gas seal cooling gas, and the temperature in the dry gas seal area obviously increase, indicating that the inlet temperature of dry gas seal directly affects the cooling effect.

The nephogram of the temperature at the axial section with x = 0.55 m is shown in Figures 24 and 25. As shown in Figure 24 and Figure 25, with the increase of the cooling flow rate of dry gas seal, the cross section temperature distribution is obviously improved. The leakage flow to the cylinder dry gas seal increases from 1.3 kg/s to 2.08 kg/s, and the temperature distribution in the cross section has no obvious change. With the increase of inlet temperature of dry gas seal, the cooling effect of shaft changes obviously, the area of high-temperature section increases, and the average temperature increases obviously.

4. CONCLUSIONS

In this paper, the numerical model of supercritical carbon dioxide turbine rotor cooling is established, and the effects of inlet temperature and flow rate of turbine dry gas seal and leakage flow rate from cylinder to dry gas seal on turbine rotor cooling are studied. The main research results are summarized as follows.

(1) With the increase of the inlet flow rate of dry gas seal gas and the leakage flow rate from cylinder to dry gas seal, the pressure difference between the inlet and outlet of each seal gas increases. When the inlet flow rate of dry gas seal gas ranges from 300 N m^3/h to 900 N m^3/h, with the leakage flow from cylinder to dry gas seal increasing from 1.3 kg/s to 2.08 kg/s, the pressure difference between inlet and outlet of each seal gas increases by 7.9% to 13.4%. The pressure difference between the inlet and outlet of each seal gas decreases with the increase of the inlet temperature of dry gas seal gas.

(2) When the inlet flow of seal gas is evenly distributed, the outlet flow distribution is not exactly the same. When the inlet flow rate of seal gas of dry gas seal is 300 N m^3/h and the leakage flow rate from cylinder to dry gas seal is 2.08 kg/s, the inlet temperature of seal gas increases from 100 to 150 °C, and the flow distribution at the outlet is basically unchanged.

(3) When the inlet temperature of sealing gas and the leakage flow from cylinder to dry gas seal are constant, the outlet temperature decreases with the increase of the inlet flow of sealing gas. Within the range of 300 N m^3/h-900 N m^3/h, the average outlet temperature increases by 3.2%−4.7% for every 200 N m^3/h increase in the inlet flow. The outlet temperature increases with the increase of leakage flow from cylinder to dry gas seal.

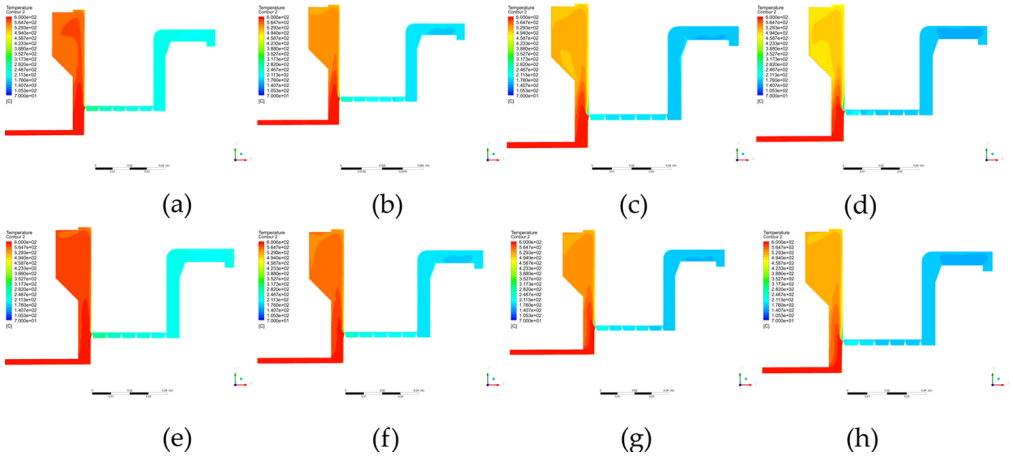

Figure 22. Temperature nephogram of fluid section z = 0 m when T_{in} = 130 °C. (a) Q_m = 1.3 kg/s, Q_v = 300 N m^3/h, T_{in} = 130 °C; (b) Q_m = 1.3 kg/s, Q_v = 500 N m^3/h, T_{in} = 130 °C; (c) Q_m = 1.3 kg/s, Q_v = 700 N m^3/h, T_{in} = 130 °C; (d) Q_m = 1.3 kg/s, Q_v = 900 N m^3/h, T_{in} = 130 °C; (e) Q_m = 2.08 kg/s, Q_v = 300 N m^3/h, T_{in} = 130 °C; (f) Q_m = 2.08 kg/s, Q_v = 500 N m^3/h, T_{in} = 130 °C; (g) Q_m = 2.08 kg/s, Q_v = 700 N m^3/h, T_{in} = 130 °C; (h) Q_m = 2.08 kg/s, Q_v = 900 N m^3/h, T_{in} = 130 °C.

https://doi.org/10.1021/acsomega.2c05531
ACS Omega 2022, 7, 39325−39334

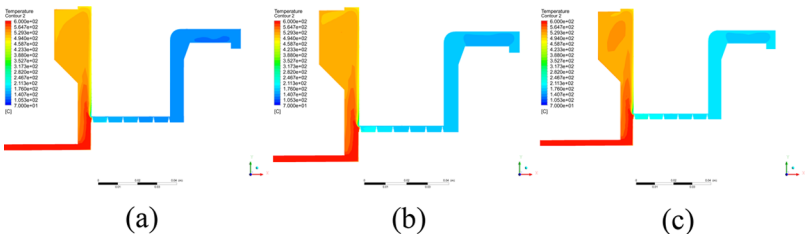

Figure 23. Temperature nephogram of fluid section z = 0 m when T_{in} = 100 °C, 130 °C, and 150 °C. (a) Q_m = 2.08 kg/s, Q_v = 900 N m^3/h, T_{in} = 100 °C; (b) Q_m = 2.08 kg/s, Q_v = 900 N m^3/h, T_{in} = 130 °C; (c) Q_m = 2.08 kg/s, Q_v = 900 N m^3/h, T_{in} = 150 °C.

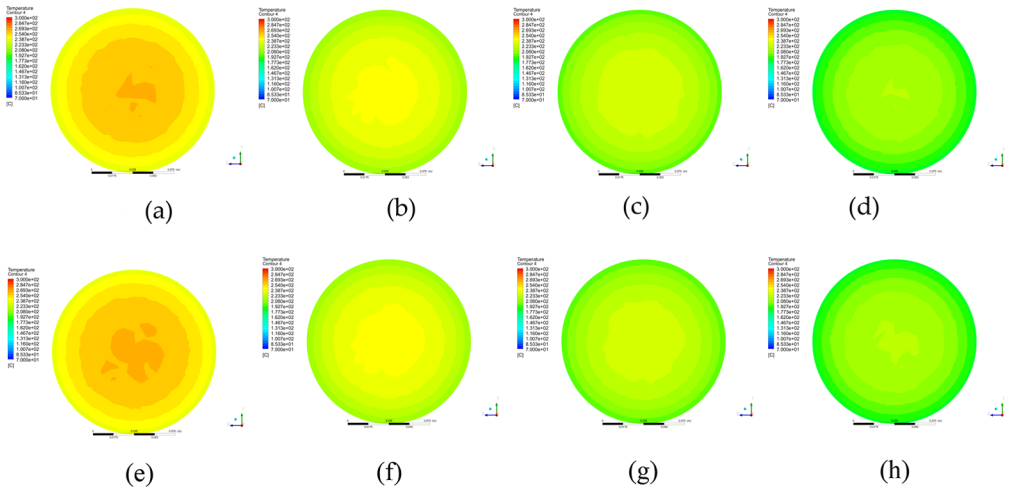

Figure 24. Temperature nephogram at x = 0.55 m axis section when T_{in} = 130 °C. (a) Q_m = 1.3 kg/s, Q_v = 300 N m^3/h, T_{in} = 130 °C; (b) Q_m = 1.3 kg/s, Q_v = 500 N m^3/h, T_{in} = 130 °C; (c) Q_m = 1.3 kg/s, Q_v = 700 N m^3/h, T_{in} = 130 °C; (d) Q_m = 1.3 kg/s, Q_v = 900 N m^3/h, T_{in} = 130 °C; (e) Q_m = 2.08 kg/s, Q_v = 300 N m^3/h, T_{in} = 130 °C; (f) Q_m = 2.08 kg/s, Q_v = 500 N m^3/h, T_{in} = 130 °C; (g) Q_m = 2.08 kg/s, Q_v = 700 N m^3/h, T_{in} = 130 °C; (h) Q_m = 2.08 kg/s, Q_v = 900 N m^3/h, T_{in} = 130 °C.

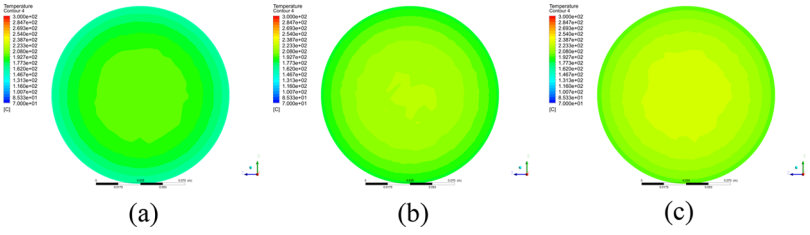

Figure 25. Temperature nephogram of x = 0.55 m axis section when T_{in} = 100, 130, and 150 °C. (a) Q_m = 2.08 kg/s, Q_v = 900 N m^3/h, T_{in} = 100 °C; (b) Q_m = 2.08 kg/s, Q_v = 900 N m^3/h, T_{in} = 130 °C; (c) Q_m = 2.08 kg/s, Q_v = 900 N m^3/h, T_{in} = 150 °C.

The outlet temperature rises with the increase of the inlet temperature of the sealing gas, and the outlet temperature rises by 3−6 °C for every 20 °C increase in the inlet temperature.

In the future, it will be necessary to verify the accuracy of the analysis results through experiments and the applicability of the conclusions in this paper in the design of higher power supercritical carbon dioxide turbines.

AUTHOR INFORMATION

Corresponding Author

Bo Wang − *Institute of Engineering Thermophysics, Chinese Academy of Sciences, Beijing 100190, People's Republic of China*; Email: wangbo@mail.etp.ac.cn

Authors

Peng Jiang − *Institute of Engineering Thermophysics, Chinese Academy of Sciences, Beijing 100190, People's Republic of China*

Yong Tian − *Institute of Engineering Thermophysics, Chinese Academy of Sciences, Beijing 100190, People's Republic of China*; orcid.org/0000-0003-1153-1643

Chaohong Guo − *Institute of Engineering Thermophysics, Chinese Academy of Sciences, Beijing 100190, People's Republic of China*

Complete contact information is available at: https://pubs.acs.org/10.1021/acsomega.2c05531

Notes

The authors declare no competing financial interest.

https://doi.org/10.1021/acsomega.2c05531
ACS Omega 2022, 7, 39325−39334

■ ACKNOWLEDGMENTS

The work was financially supported by the National Natural Science Foundation of China (Grant No. 52176090 and No. 52006216).

■ NOMENCLATURE

Q_m	Mass flow rate (kg/s)
T_{outave}	Average outlet temperature (°C)
Q_v	Volume flow rate (Nm^3/h)
P_{out}	discharge pressure (MPa)
T_{out}	Outlet temperature (°C)
T_s	Average temperature of rotor section (°C)
T_w	Average temperature of rotor wall (°C)
T	Temperature (°C)
T_{wall3}	Surface temperature of the rotor at the installation position of the bearing (°C)
ΔP_{ave}	Average pressure difference (MPa)
n	Rotation speed (rpm)
T_{in}	Dry gas seal inlet temperature (°C)
Q_{out}	Outlet mass flow rate (kg/s)
ΔP	Pressure difference (MPa)
P_{out}	Outlet static pressure (MPa)
T_{wall1}	Inlet temperature on the wall1 (°C)
T_{wall2}	Inlet temperature on the wall2 (°C)

■ REFERENCES

(1) Feher, E. G. Supercritical thermodynamic power cycle. In Proceeding of the IECEC 1967, Miami Beach, FL, August 13−17, 1967.
(2) Ehsan, M. M.; Guan, Z. Q.; Klimenko, A. Y.; Wang, X. R. Design and comparison of direct and indirect cooling system for 25MW solar power plant operated with supercritical CO_2 cycle. *Energy Convers. Manage.* **2018**, *168*, 611−28.
(3) Mohammadi, K.; Ellingwood, K.; Powell, K. A novel triple power cycle featuring a gas turbine cycle with supercritical carbon dioxide and organic Rankine cycles: Thermoeconomic analysis and optimization. *Energy Conversion and Management* **2020**, *220*, 113123.
(4) Saeed, M.; Kim, M.-H. Analysis of a recompression supercritical carbon dioxide power cycle with an integrated turbine design/optimization algorithm. *Energy* **2018**, *165*, 93−111.
(5) Reyes-Belmonte, M. A.; Sebastian, A.; Romero, M.; Gonzalez-Aguilar, J. Optimization of a recompression supercritical carbon dioxide cycle for an innovative central receiver solar power plant. *Energy* **2016**, *112*, 17−27.
(6) Zhou, A.; Song, J.; Li, X.; Ren, X.; Gu, C. Aerodynamic design and numerical analysis of a radial inflow turbine for the supercritical carbon dioxide Brayton cycle. *Appl. Therm. Eng.* **2018**, *132*, 245−255.
(7) Zhang, H.; Zhao, H.; Deng, Q.; Feng, Z.Aerothermodynamic design and numerical investigation of supercritical carbon dioxide turbine. Proceedings of ASME Turbo Expo 2015: Turbine Technical Conference and Exposition GT2015; June 15−19, 2015, Montréal, Canada, GT2015−42619.
(8) Uusitalo, A.; Gronman, A. Analysis of radial inflow turbine losses operating with supercritical carbon dioxide. *Energies* **2021**, *14*, 3561.
(9) Odabaee, M.; Sauret, E.; Hooman, K. CFD simulation of a supercritical carbon dioxide radial-inflow turbine, comparing the results of using real gas equation of estate and real gas property file. *Appl. Mech. Mater.* **2016**, *846*, 85−90.
(10) Luo, D.; Liu, Y.; Sun, X.; Huang, D. The design and analysis of supercritical carbon dioxide centrifugal turbine. *Appl. Therm. Eng.* **2017**, *127* (25), 527−535.
(11) Yan, R.; Chen, H.; Zhang, W.; Hong, X.; Bao, X.; Ding, X. Calculation and verification of flow field in supercritical carbon dioxide dry gas seal based on turbulent adiabatic flow model. *Tribol. Int.* **2022**, *165*, 107275.
(12) Thatte, A.; Dheeradhada, V. Coupled physics performance predictions and risk assessment for dry gas seal operating in MW-scale supercritical CO_2 turbine. *Proc. ASME Turbo Expo 201* **2016**, GT2014−57670.
(13) Yuan, T.; Li, Z.; Li, J. Design and analysis of cooling structure for dry gas seal chamber of supercritical carbon dioxide turbine shaft end. *Proc. ASME Turbo Expo 2021* **2021**, *Virtual*, GT2021−59177.
(14) Laxander, A.; Fesl, A.; Hellmig, B.Development and testing of dry gas seals for turbomachinery in multiphase CO_2 applications. 3rd European supercritical CO_2 Conference, September 19−20, 2019, Paris, France, 2019-sCO_2. eu-116.
(15) SI, H.; CAO, L.; Chen, D. Dynamic characteristics of supercritical carbon dioxide (SCO_2) seal influenced by multiple factors. *Tribol. Int.* **2021**, *162*, 107131.
(16) Du, Q.; Gao, K.; Zhang, D.; Xie, Y. Effects of grooved ring rotation and working fluid on the performance of dry gas seal. *Int. J. Heat Mass Transfer* **2018**, *126*, 1323−1332.
(17) Muhammad, H. A.; Lee, B.; Imran, M.; Cho, J.; Cho, J.; Roh, C.; Lee, G.; Shin, H.; Sultan, H.; Baik, Y.-J. Investigating supercritical carbon dioxide power cycles and the potential of improvement of turbine leakage characteristics via a barrier gas. *Appl. Therm. Eng.* **2021**, *188*, 116601.
(18) Wu, J.; Zhao, X.; Zhao, Z.; Dai, L.; Lao, X.; Lv, W. Numerical study on sealing performance of supercritical carbon dioxide compressor dry gas seal. *IOP Conf. Series: Earth and Environmental Science* **2020**, *461*, 012046.
(19) Fairuz Zakariya, M.; Jahn, H. J. I.Performance of supercritical CO_2 dry gas seals near the critical point. Proceedings of ASME Turbo Expo 2016: Turbomachinery Technical Conference and Exposition GT2016 June 13−17, 2016, Seoul, South Korea, GT2016−56537.
(20) Du, Q.; Zhang, D. Research on the performance of supercritical CO_2 dry gas seal with different deep spiral groove. *J. Therm. Sci.* **2019**, *28*, 547−558.
(21) Fairuz Zakariya, M. Simulation and development of dry gas seal for supercritical CO_2 carbon dioxide. Ph.D. Thesis, The University of Queensland, 2017.
(22) Fairuz, Z.M.; Jahn, I.; Abdul-Rahman, R. The effect of convection area on the deformation of dry gas seal operating with supercritical CO_2. *Tribol. Int.* **2019**, *137*, 349−365.
(23) Jiang, P.; Wang, B.; Tian, Y.; Xu, X.; Zhao, L. Design of a supercritical CO_2 compressor for use in a 1 MWe power cycle. *ACS Omega* **2021**, *6*, 33769−33778.
(24) *Ansys Fluent User Guide Release, 16*; Ansys Inc., 2015.
(25) Lemmon, E; Huber, M; McLinden, M.NIST p fluid thermodynamic and transport properties-REFPROP, version 9.0. Tech. Rep. *Physical and Chemical Properties Division*; National Institute Of Standards and Technology, 2010.
(26) Span, R.; Wagner, W. A new equation of state for carbon dioxide covering the fluid region from triple point temperature to 1100K at pressure up to 800 MPa. *J. Phys. Chem. Ref. Data* **1996**, *25*, 1509−1596.

https://doi.org/10.1021/acsomega.2c05531
ACS Omega 2022, 7, 39325−39334